Physica Scripta

OPEN ACCESS

RECEIVED
23 December 2023

REVISED
30 April 2024

ACCEPTED FOR PUBLICATION
9 May 2024

PUBLISHED
23 May 2024

PAPER

Balanced travelling-wave parametric amplifiers for practical applications

J C Longden , J Navarro Montilla and B-K Tan

Department of Physics (Astrophysics), University of Oxford, Denys Wilkinson Building, Keble Road, Oxford OX1 3RH, United Kingdom

E-mail: joseph.longden@physics.ox.ac.uk **and** boonkok.tan@physics.ox.ax.uk

Keywords: parametric amplifier, travelling-wave, kinetic inductance, phase-control, wave mixing, balanced amplifier

Abstract

The development of superconducting travelling-wave parametric amplifiers (TWPAs) over the past decade has highlighted their potential as low-noise amplifiers for use in fundamental physics experiments and industrial applications. However, practical challenges, including signal-idler contamination, complex pump injection and cancellation, impedance mismatch, and the reciprocal nature of the device, have made it challenging to deploy TWPAs in real-world applications. In this paper, we introduce an innovative solution to these issues through phase-controlled balanced-TWPA architectures. These architectures involve placing two TWPAs in parallel between a pair of broadband couplers. By carefully controlling the phases of the tones propagating along the TWPAs, we can effectively separate the signal and idler tones, as well as the pump(s), using a straightforward injection and cancellation mechanism. The balanced-TWPA architecture offers versatility and flexibility, as it can be reconfigured either intrinsically or externally to suit different application needs. In this manuscript, we provide a comprehensive discussion of the working principles of the balanced-TWPA, including various configurations designed to meet diverse application requirements. We also present the expected gain-bandwidth products in comparison to traditional TWPAs and conduct tolerance analysis to demonstrate the feasibility and advantages of the balanced-TWPA architecture. By addressing the practical challenges associated with TWPAs, the balanced-TWPA architecture represents a promising advancement in the field, offering a more practical and adaptable solution for a wide range of applications.

1. Introduction

Superconducting travelling-wave parametric amplifiers (TWPAs) [1–3] are quantum devices that achieve high gain over broad bandwidth by efficiently transferring power from a strong 'pump wave to a detected weak 'signal wave in a non-linear transmission line, created by either embedding Josephson junctions along a transmission line [4–7] or by exploiting the non-linear kinetic inductance of high-gap superconducting thin films [8–12]. During the amplification process, an idler tone is generated to preserve the energy and momentum of the system. TWPAs have been shown to achieve quantum-limited noise performance, ideal for the readout of highly sensitive cryogenic detection systems including astronomical receivers [13–15], dark matter search experiments [16–18], and quantum computers [19–21].

Despite their potential, the implementation of TWPAs in real experiments has been limited due to a number of practical obstacles. The first generation of TWPAs operating in the degenerate-pump four-wave mixing (DP-4WM) mode [1, 22] exhibited undesirable characteristics, such as a large zero-gain gap at the centre of the gain profile and gain roll-off. These issues have been addressed in second-generation devices, which operate the TWPA in either the dual-pump non-degenerate-pump four-wave mixing (NP-4WM) mode [23, 24] or the DC-induced three-wave mixing (DC-3WM) regime [2, 11]. Despite these improvements, however, TWPAs still face challenges that hinder their widespread use beyond superconducting quantum computing fields e.g. astronomical receivers, dark matter search, etc. These include the contamination between the signal and idler

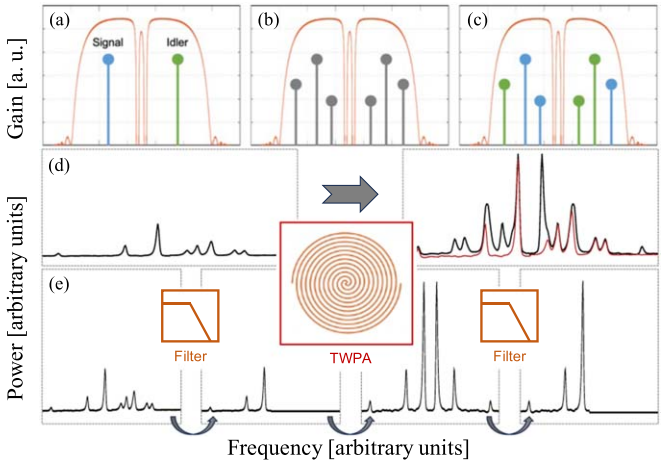

Figure 1. Examples highlighting the contamination of the amplified signal by the idler tone. (a) Output spectrum from TWPA, highlighting the amplified signal and generated idler. (b) Output spectrum from TWPA with more input tones, highlighting how without prior knowledge, it is impossible to distinguish between the amplified signal and generated idler tones. (c) Same spectrum as (b), now with the signal and idler tones colour coded to highlighting particular input tones. In (a)–(c), the red line denotes an example D-4WM signal gain curve, showing that for a given signal-idler pair, one will be in each half of the gain profile. (d) Similar illustration with a continuous spectrum profile (black), showing the TWPA amplified output fails to recover the actual input profile (red curve). In the right hand figure, the black curve shows the measured output spectrum, and the red curve shows the output spectrum of the amplified signal only. (e) Possible idler removal technique, whereby half the spectrum is filtered before and after amplification.

tones, the need for complex experimental setups to inject and cancel the pump tones for proper operation, impedance mismatches, and their unity-gain reverse transmission ($|S_{12}|$), which makes them susceptible to 'back-radiation' that could disrupt sensitive devices under test (DUTs), such as qubits. In this paper, we propose a simple and elegant solution to address all of these issues while maintaining the quantum-limited, broadband, and high-gain performance of TWPAs. It is important to note that this solution can be applied to various TWPA variants, including kinetic inductance (KI-) [1, 9–12], Josephson junction (J-) [4–7], and superconducting quantum interferometric device (SQUID-)TWPAs [3, 25].

2. Current challenges in operating a TWPA in realistic situation

In broadband TWPA devices, the idler tone produced during the parametric amplification process is generated at a different frequency to the incident signal tone. As shown in figure 1(a), the signal and idler frequencies are located symmetrically on opposite sides of the centre frequency of the gain profile. If the input signal comprises a spectrum of different frequencies on both sides of the amplifier centre frequency, then the generated idler terms would overlap with amplified signal tones at the same frequency and distort the amplified signal spectrum. Consider the simple set of TWPA-amplified detected tones that is shown in figure 1(b) and comprises six peaks: three being the amplified signals and the other three the generated idlers. Assuming no prior knowledge of the input tones (as in most cases), it is impossible to distinguish between the desired signal spectrum and the unwanted idler contamination i.e., the input spectrum cannot be recovered from the output spectrum (see figure 1(c)). Figure 1(d) illustrates the same concern with a continuous spectrum profile to further highlight the issue i.e., the amplified output from the TWPA fails to reproduce the profile of the input spectrum. This signal-idler contamination issue renders the TWPA unusable without additional filtering before and after the TWPA, or via the use of other complicated setups involving diplexers etc. As shown in figure 1(e), an incoming signal spectrum can be filtered prior to amplification such that only signal frequencies at the lower-half of the operational band are amplified by the TWPA[1], which prevents any components higher than the centre frequency from generating an idler tone in the lower half of the spectrum. Further filtering or diplexing post-amplification is also required to remove the higher frequency idler generated by the lower frequency signal to recover the amplified spectrum. Whilst this technique solves the signal-idler contamination problem, it unavoidably halves the operational bandwidth of the TWPA, which is unideal.

Another significant challenge in the practical operation of a TWPA is the complexity of the required experimental setup. As illustrated in figure 2, a typical experimental arrangement for operating a NP-4WM TWPA [24] involves a multitude of additional components such as directional couplers, power dividers, variable attenuators, and phase shifters, which are essential for combining the pump and signal tones before injecting

[1] The same analysis applied to the case where the desired signal is restricted to the upper half of the band.

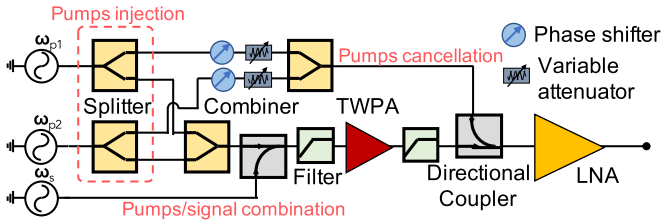

Figure 2. Complicated experimental setup required to operate a NP-4WM TWPA, but most components are still required for other TWPA wave mixing regimes.

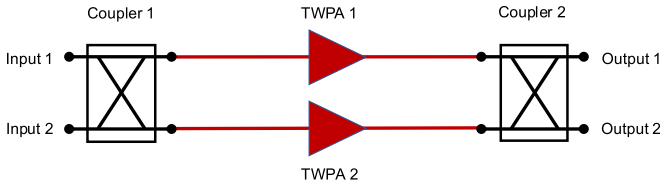

Figure 3. Schematic of a parallel-TWPA architecture, showing a pair of TWPAs placed in parallel between a pair of generic RF couplers.

them into the TWPA and subsequently cancelling the pump tones post-amplification. These added components are often physically larger than the TWPA itself and must be mounted at various cryogenic stages, consuming valuable space within the cryostat. Furthermore, pump cancellation necessitates additional coaxial lines running down to the cold stages of the cryostat, increasing the thermal load. Scaling experimental setups to array applications, therefore, becomes particularly challenging, as the growing number of components and coaxial cables places an unsustainable thermal and power load on the cryostat. Therefore, simplifying the integration of TWPAs into cryogenic experimental setups using the most straightforward operational module is imperative.

A further issue with existing TWPA operation is their (ideally) unity-gain $|S_{12}|$, which allows radiation to pass through them in the reverse direction. In a conventional transistor amplifier, the magnitude of the reverse transmission, $|S_{12}|$, is typically extremely small. Consequently, any back-radiation from components further down the signal chain is effectively prevented from radiating backwards and disrupting a potentially sensitive DUT. With a TWPA, however, the $|S_{12}|$ is nominally the same as the un-pumped (without pump tone) $|S_{21}|$, implying that any back-radiation may be transmitted through the TWPA and potentially disturb the DUT. Preventing this scenario often requires the use of an additional circulator, which introduces additional thermal, spatial, and financial costs. It also imposes bandwidth restrictions and introduces losses.

3. Parallel-TWPA architecture

Our proposed solution to address these challenges involves the use of a parallel-TWPA architecture [26], as illustrated in figure 3. This configuration consists of a pair of TWPA devices connected in parallel between a pair of generic RF couplers, typically equipped with two-input and two-output ports. Certain RF couplers, such as quadrature hybrids, introduce a phase shift to the propagating tones before and after they enter the TWPAs. By carefully controlling the phases of the various tones passing through the TWPAs, it is possible to engineer constructive and destructive interference at the output ports. This engineering allows for the clean separation of the pump, signal, and idler tones, effectively resolving the challenges described earlier. A similar architecture has previously been demonstrated [27] using a pair of narrow-band Josephson parametric amplifiers (JPAs) [17, 28–31] and a single RF coupler, however, we extend the idea here to TWPAs to exploit their wideband performance.

In the following sections, we present a series of parallel-TWPA examples, which utilise a pair of KITWPAs. The KITWPA design comprises a 42 cm long, 50 Ω 'fishbone'-style CPW transmission line patterned into a 100 nm thick titanium nitride (TiN) film, which is deposited onto a 500 μm thick sapphire substrate. Periodic impedance loadings are made to the transmission line every 460 μm to achieve the desired dispersion engineering, and the designed pump frequency is 6.41 GHz. Full details of the KITWPA device are presented in [32]. The transmission and gain performance are simulated using the rigorous modelling technique described in [22], and are presented in figure 4.

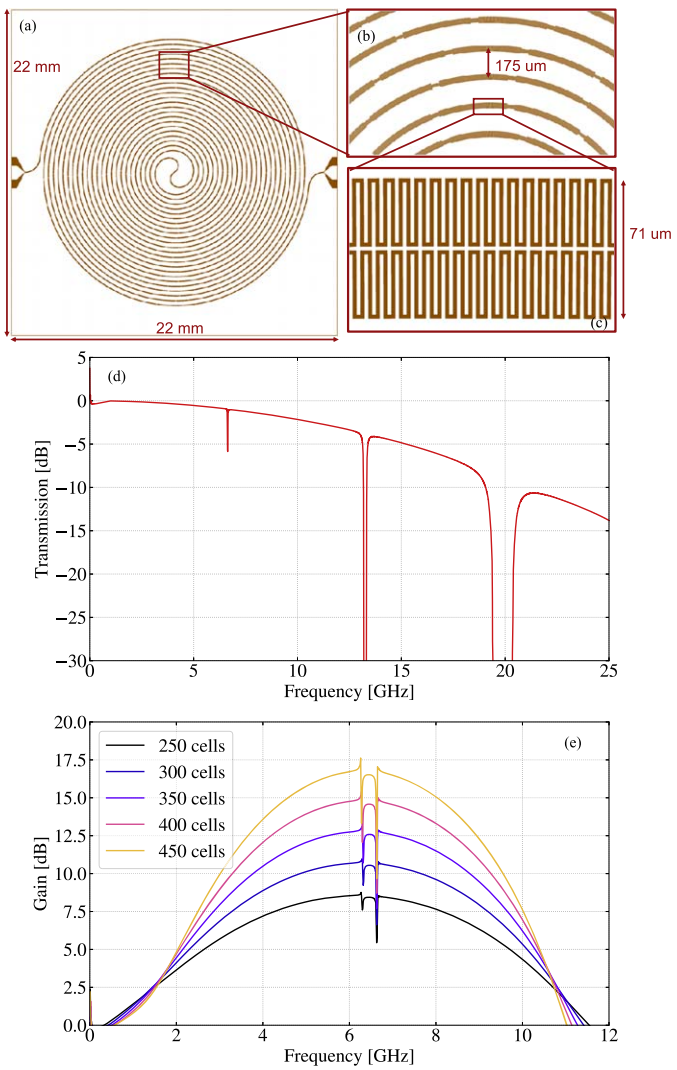

Figure 4. (a) CAD image of KITWPA design, showing 42 cm long CPW transmission line wound into a double spiral pattern to fit onto a 22 mm by 22 mm chip. The dark regions show where the TiN has been removed. (b) Zoom in of transmission line in (a), showing periodic loading structure. (c) Zoom in of transmission line in (b), showing the 'fishbone' structure of the CPW. (d) Simulated un-pumped transmission spectrum of KITWPA device. (e) Simulated gain profiles of KITWPA device for various numbers of unit cells at a pump frequency of 6.41 GHz, and a pump current of 0.15 I_*, where I_* is the term that sets the scale of the non-linearity of the kinetic inductance.

Central to the successful operation of this parallel-TWPA architecture is the phase control of the propagating tones. Consider the total current passing along a TWPA, as described by the ansatz in,

$$I(z,\,t) = \sum_j I_j = \sum_j A_j(z) e^{\gamma_j z + i(-\omega_j t + \delta_j)} + c.c.\,, \tag{1}$$

which is formed by the sum of j current components propagating along the transmission line, where A_j is the slowly-varying complex amplitude of the component, ω_j is the (angular) frequency of the component, $\gamma_j = \alpha_j + i\beta_j$ is the complex propagation constant, δ_j is the arbitrary initial phase of the jth current component, z is the position along the transmission line, t is time, and *c. c.* denotes the complex conjugate. In most formulations of the coupled-mode equations (CMEs) reported in the literature, δ_j is not explicitly included and it is assumed that $\delta_j = 0$. To preserve generality, however, we explicitly include δ_j in our CMEs and absorb it into the complex amplitude of the current,

$$\begin{aligned} I(z,\,t) &= \sum_j A_j(z) e^{\gamma_j z + i(-\omega_j t + \delta_j)} + c.c. \\ &= \sum_j A_j(z) e^{i\delta_j} e^{\gamma_j z - i\omega_j t} + c.c. \\ &= \sum_j A_j'(z) e^{\gamma_j z - i\omega_j t} + c.c.\,, \end{aligned} \tag{2}$$

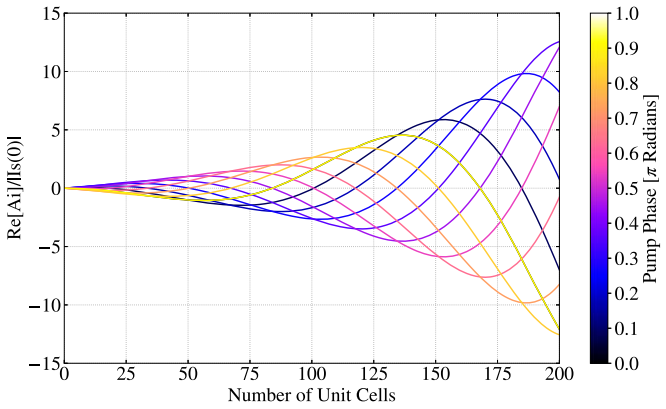

Figure 5. The real component of the idler amplitude, $\Re(A_i)$, normalised to the amplitude of the initial signal current, $|I_s(0)|$, as the phase of the pump tone is swept.

where, $A_j'(z) = A_j(z)e^{i\delta_j}$. Since our CMEs deal with complex current values, the initial conditions for the propagating tones must be provided in the complex form as well i.e., $I_j(0) \rightarrow I_j(0)e^{i\delta_j}$. With this complex framework, we explore the phase relations of the tones propagating along a DP-4WM TWPA as an example, although the same analysis can be easily extended to other wave mixing regimes as well.

In the following, we investigate how changing the initial phase of one of the tones propagating along a TWPA effects the behaviour of the other tones. Figure 5 shows the real part of the idler amplitude, $\Re(A_i)$, as a function of position, z, along the length of a TWPA, which has been calculated by numerically solving the CMEs for a lossless TWPA operating in the DP-4WM mode,

$$\frac{dA_\mathrm{p}}{dz} = -\frac{i\beta_\mathrm{p}}{8I_*^2}[(|A_\mathrm{p}|^2 + 2\,|A_\mathrm{s}|^2 + 2\,|A_\mathrm{i}|^2)A_\mathrm{p} + 2A_\mathrm{i}A_\mathrm{s}A_\mathrm{p}^* e^{-i\Delta_\beta^{(\mathrm{D4})}z}] \tag{3a}$$

$$\frac{dA_\mathrm{s}}{dz} = -\frac{i\beta_\mathrm{s}}{8I_*^2}[(|A_\mathrm{s}|^2 + 2\,|A_\mathrm{i}|^2 + 2\,|A_\mathrm{p}|^2)A_\mathrm{s} + A_\mathrm{i}^* A_\mathrm{p}^2 e^{i\Delta_\beta^{(\mathrm{D4})}z}] \tag{3b}$$

$$\frac{dA_\mathrm{i}}{dz} = -\frac{i\beta_\mathrm{i}^2}{8I_*^2}[(|A_\mathrm{i}|^2 + 2\,|A_\mathrm{p}|^2 + 2\,|A_\mathrm{s}|^2)A_\mathrm{i} + A_\mathrm{s}^* A_\mathrm{p}^2 e^{i\Delta_\beta^{(\mathrm{D4})}z}], \tag{3c}$$

where $\Delta_\beta^{(\mathrm{D4})} = \beta_\mathrm{s} + \beta_\mathrm{i} - 2\beta_\mathrm{p}$ and $\beta_j = \Im(\gamma_j)$. As stated, the slowly-varying amplitude of each component, $A_j(z)$, is a complex value, therefore, we can modify the initial phase of, say, the pump tone and see how this effects the complex amplitude of the idler tone, $A_i(z)$.

In figure 5 we, therefore, calculate and plot the real part of the idler tone for various arbitrary initial phases of the pump tone. Whilst the magnitude of the idler component remains unchanged as the initial pump phase is varied, as indicated by the positive envelope function of each of the curves, the phase of the idler tone shifts with the initial pump phase. The fact that the magnitude of the idler is unaffected by the pump's phase shift is expected, as any (conversion) gain should not be influenced by the initial pump phase. The shift in the phase of the idler tone is interesting though, as it suggests that we are able to control it by controlling the phase of the pump externally.

This behaviour is further explored in figure 6, which shows how the idler phase varies as a function of the initial pump phase for different initial signal phases. From this plot, we clearly see that shifting the pump phase by δ_p will shift the idler phase by $2\delta_p$, and that shifting the signal phase by δ_s will shift the idler phase by $-\delta_s$ i.e.,

$$\delta_i = 2\delta_p - \delta_s. \tag{4}$$

This relation between the phase shifts is important, as it means that it is now possible to control the idler tone independently from the signal tone by tuning the phase of the pump tone externally. We will now demonstrate how this can be utilised to provide solutions to the various issues described previously.

Figure 7(a) shows a pair of TWPAs operating in the DP-4WM mode between a pair of in-phase Wilkinson power dividers/combiners. A pump tone at a certain frequency is split with equal magnitude and injected into each TWPA, with the pump tone in the bottom arm having a $\frac{\pi}{2}$ radian phase shift relative to the pump tone in the top arm. As we can see from figure 7(a) and equation (4), a $\frac{\pi}{2}$ radian phase shift in the pump tone results in a π radian phase shift to the idler tone in the lower TWPA arm relative to the upper arm, which means that upon recombination by a second power combiner, the idler tones are now in anti-phase, hence they cancel. Specifically, the energy of the two idler tones is dissipated across the internal resistive element of the second Wilkinson combiner as heat. This idler dissipation means that only the signal and the pump are present at the

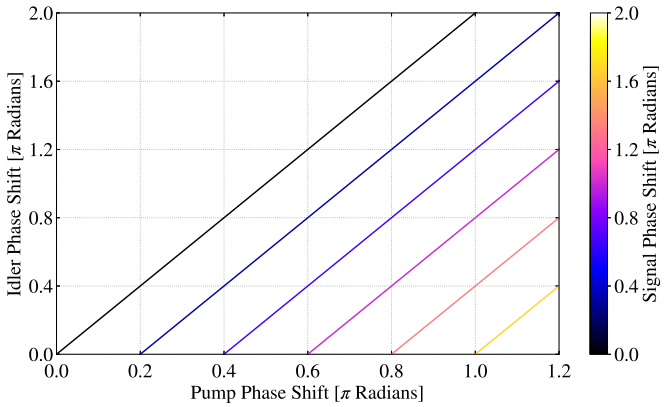

Figure 6. The idler phase shift, δ_i, as a function of the initial pump phase, δ_p, and signal phase shift, δ_s.

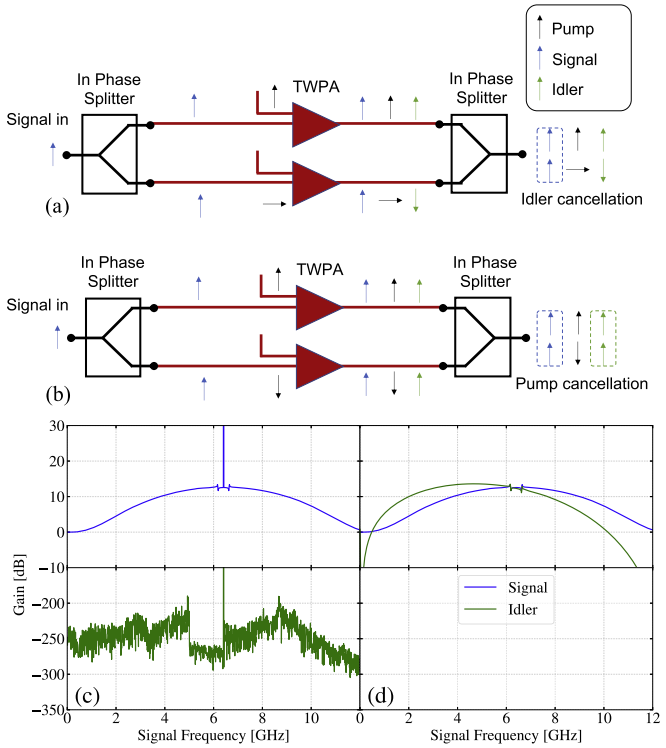

Figure 7. Circuit diagrams of a DP-4WM parallel-TWPA with in-phase Wilkinson power dividers/combiners. The blue, black, and green arrows represent the signal, pump and idler, respectively, and the direction of each arrow indicates the relative phase of each tone, with up-pointing arrow set at zero radian. (a) The pump tone of the bottom arm is shifted by $\frac{\pi}{2}$ radians relative to the top arm, leading the idler tones being π radians out-of-phase at the output, and thus cancelling. (b) The identical setup to (a) but with the pump tone feeding the bottom arm now being π radians out-of-phase relative to the top arm, leading to pump cancellation. (c) Simulated gain profiles of the output tones for parallel-TWPA configuration shown in (a). (d) Similarly for configuration shown in (b).

output, solving the signal-idler contamination problem described in figure 1. It should be additionally noted that due to the two pump tones being $\frac{\pi}{2}$ radians out-of-phase, some of their energy will also be dissipated across the internal resistive element as heat.

The signal-idler contamination is not the only obstacle that can be reconciled using the parallel-TWPA architecture. If we use the identical setup to the previous analysis but now shift the pump tone in the lower TWPA by a further $\frac{\pi}{2}$ radians such that the pump tones in each TWPA are now π radians out-of-phase, the setup can be operated in a regime such that the two pump tones are now dissipated by the second Wilkinson combiner and, hence, removed at the output port, as illustrated in figure 7(b). The advantage of this configuration is that we can now easily remove the pump from the subsequent amplified signal spectrum without the need for additional coaxial lines and RF components, as the couplers can be easily integrated with the TWPAs in the same block.

Of course, in practice the dissipation of the cancelled tones over the resistive element of the second Wilkinson combiner will cause significant heating of the parallel-TWPA device at cryogenic temperatures, which could drastically alter and degrade the behaviour of the parallel-TWPA system. We include this architecture here, however, as it provides a simpler configuration to discuss the general operational principles of parallel-TWPAs, before we proceed to more complex configurations in subsequent sections that eliminate this issue.

To verify the behaviour of the parallel-TWPA architecture shown in figures 7(a)–(b), we simulate the gain profiles of the parallel-TWPA, by appropriately initiating the phases of the input tones, before separately solving the CMEs for each TWPA in the parallel-TWPA setup using the methodology described in [22]. The output tones from each TWPA are then summed together and used to calculate the gain of each tone, relative to their initial value. For the idler tone, we calculate the gain relative to the input signal tone, hence it is technically a conversion gain, but is referred to here simply as idler gain. The results are shown in figure 7(c) for the configuration shown in figures 7(a), and 7(d) for 7(b). From these plots, it is clear that we managed to fully suppress the idler tone for the configuration shown in figure 7(a) and that the pump is completely cancelled at the output for figure 7(b) setup.

The above examples demonstrate the operational principle and functionality of the simplest balanced-TWPA configuration (named such, as the architecture and operational principle is similar to the conventional balanced amplifier and the balanced mixer [33, 34]). However, we stress that the same parallel-TWPA architecture is actually very versatile and flexible. The in-phase splitter can be replaced with any 3- or 4-port coupler and switched between different operational modes *in situ* simply by externally controlling the phase difference between the pump tones etc., to cater for different applications.

4. Balanced-TWPAs

The simple scheme shown in previous section to explain the principle of the balanced-TWPA seems to imply that it can only solve one issue at a time, but this is in fact not the case. In this section, we describe a few more configurations that can be used in practice, to demonstrate the versatility of the technique and to show that there are indeed schemes that can solve all of the above issues, hence an ideal TWPA. Given that all these configurations make use of the same phase-controlling technique, only a brief description is given for each example.

As previously discussed, using a 3-port power splitter is impractical due to the significant power dissipation over the internal resistive element of the coupler, which can lead to heating of the cryogenic environment that an experimental setup is housed in. A better option would be to use 4-port quadrature hybrids. Figure 8(a) shows a similar setup to those shown in figures 7(a)–(b), except the signal is now fed into one input port of a quadrature hybrid, with the other input port being terminated. Two in-phase pump tones are injected into the parallel-TWPAs and all subsequent output tones are recombined by a second quadrature hybrid. Figure 8(b) shows the simulation results for this configuration. The power at the output ports of the hybrid, P_{out}, are given by,

$$P_{\text{out}}^{(\text{Port 1})} = \frac{1}{\sqrt{2}}\left(P_{\text{in}}^{(\text{Port 1})}e^{-i\frac{\pi}{2}} + P_{\text{in}}^{(\text{Port 2})}e^{-i\pi}\right) \tag{5a}$$

$$P_{\text{out}}^{(\text{Port 2})} = \frac{1}{\sqrt{2}}\left(P_{\text{in}}^{(\text{Port 1})}e^{-i\pi} + P_{\text{in}}^{(\text{Port 2})}e^{-i\frac{\pi}{2}}\right), \tag{5b}$$

where P_{in} denotes the power at the input port of the hybrid.

In this setup, not only is the idler tone removed from the signal output port, but it is diverted separately to its own output port i.e., we have an idler separation scheme rather than simply a cancellation scheme. This is advantageous because as the frequency relation between the signal and idler is known, the idler can in fact be used post-amplification e.g. converting back to the signal frequency range by cascading a pair of balanced-TWPA in series to further increase the gain. Additionally, by routing the separated idler tone outside the cryostat via a separate RF line, its power is not dissipated at the cold stage of the cryostat, which minimises the risk of unwanted heating.

As discussed previously, the reciprocity of a TWPA means that any back-radiation from subsequent components, such as a low-noise amplifier (LNA) with a poor $|S_{11}|$ can disturb the sensitive DUT before the TWPA. This is the same for the balanced-TWPA if the output signal is measured, as any back-radiation will be transmitted back to the signal input port (see e.g. Figure 8). If we instead read out the output idler tone and terminate the output signal port, we would be able to create a non-reciprocity in the balanced-TWPA, where any back-radiation emitted into the output idler port will be transmitted back to the terminated input port, rather than the DUT, without the need for additional circulators. We named this the 'reverse-isolating mode' of the balanced-TWPA. It is clear that the configuration shown in figure 8 also allows for any impedance mismatch

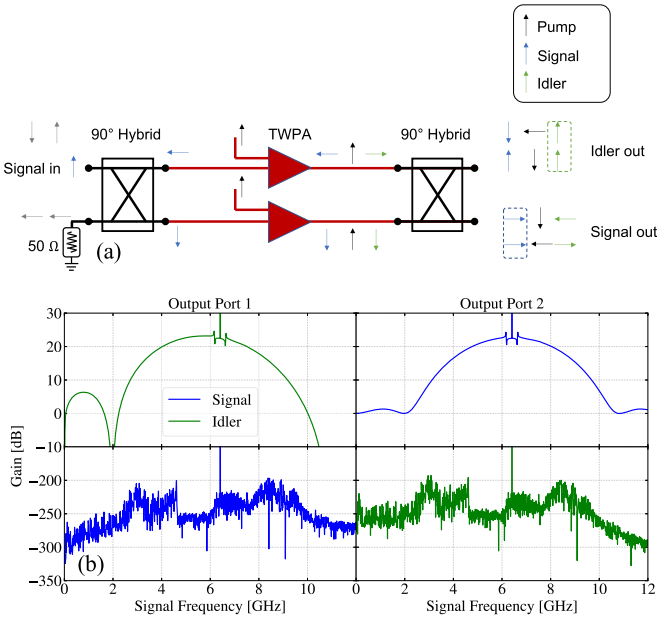

Figure 8. (a) Circuit diagram of a DP-4WM balanced-TWPA with quadrature hybrids. This setup uses a quadrature hybrid to split the incoming signal with a phase difference of $\frac{\pi}{2}$ radians between the two arms Injecting in-phase pump tones into the TWPAs results in the signal and idler tones exiting different ports of the parallel-TWPA, thus being separated. Additionally, any reflected power at the input of the TWPA will be terminated at the unused input port (grey arrows). (b) Simulated gain profiles of the output tones at each output ports.

between the TWPAs and external circuitry to be mitigated, as any reflections from the input ports of the amplifiers will be reflected to the terminated input port instead of to the DUT.

The configuration shown in figure 8 resolves the signal-idler contamination issue, but the pump injection scheme remains complicated, as the pump still needs to be injected into both TWPAs independently in the traditional way. Instead of terminating one of the hybrid input ports, the signal and pump can instead be injected into the separate input ports of the hybrid, which is shown in figure 9(a), with the corresponding simulation results shown in figure 9(b). This drastically simplifies the pump injection and cancellation mechanisms, removing the need for additional couplers, phase shifters, variable attenuators, and additional RF lines running into the cryostat, as well as freeing space within the cryostat. The added advantage of separating out the pump tone from the signal is that the output of the barely-depleted pump from one balanced-TWPA can now be subsequently used to pump another, providing a possible way of creating an array of TWPAs with just one pump line, as illustrated in figure 10. Alternatively, the output pump can simply be routed out of the cryostat via a separate RF line to minimise its power dissipation.

An important practical consideration of this configuration is the finite isolation between the signal input port and the pump input port, which means that some of the coupled pump tone will leak from the pump input port to the signal input port and back to the DUT. Hybrid port isolation is typically around 20 dB, so if the pump power is 40 dB higher than the input signal power, which is not uncommon for a TWPA, then there is a potential leakage pump tone back-acting on the input that is roughly 20 dB stronger than the signal tone. It should be noted, however, that this is no different to the traditional way of operating a TWPA, which uses a directional coupler placed before the TWPA to couple-in the pump tone, as well as a second coupler placed after the TWPA to cancel the pump tone following amplification. Directional couplers also have a finite port isolation of a similar magnitude to quadrature hybrids, hence they can also reverse-couple the pump tone to the DUT with a high magnitude. Therefore, whilst the balanced-TWPA configuration may still require certain components like circulators in practical applications, this is no worse than the traditional case, with the added advantage that the balanced-TWPA can integrate many of the additional components onto a single chip and eliminate the need for some of them, such as phase shifters and variable attenuators, altogether.

All of the previous examples have focused on the DP-4WM TWPAs, but the same can be applied to NP-4WM TWPAs. The phase relation for NP-4WM mode can be summarised by,

$$\delta_i = \delta_{p1} + \delta_{p2} - \delta_s, \tag{6}$$

and we can clearly see that we now have three separate phase shifts that we can adjust to control the idler tone.

Figure 11(a) shows the balanced-NP4WM-TWPA capable of signal and idler separation with the corresponding outputs shown in figure 11(b). The physical configuration is identical to that shown in figure 9,

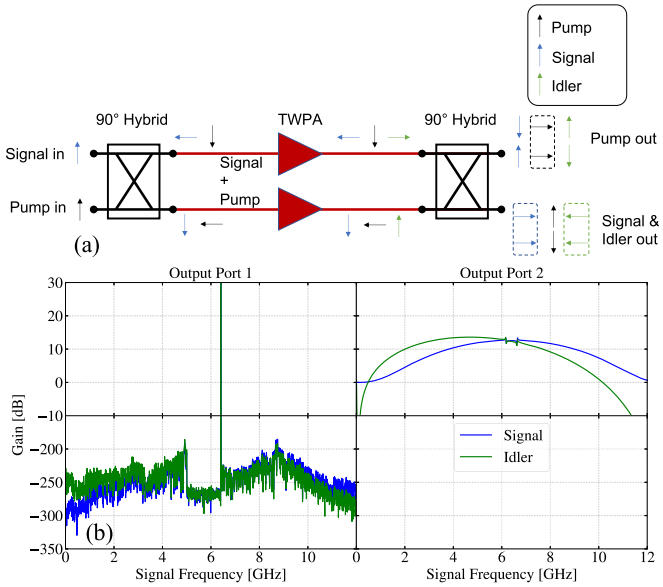

Figure 9. (a) Circuit diagram of a DP-4WM parallel-TWPA with quadrature hybrids. This setup involves injecting the signal and pump tones into separate input ports of the first hybrid, which creates different relative phases at each TWPA. Combining the resultant signals at the second hybrid results in the pump exiting at one port and the signal and idler exiting at the other. (b) Simulated gain profiles of the output tones at each output port.

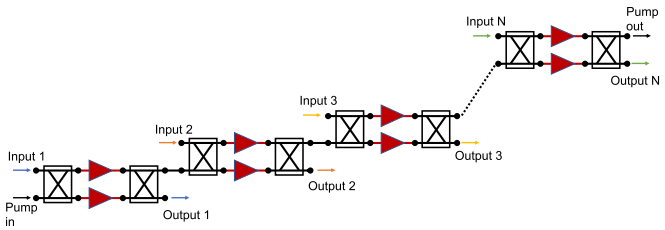

Figure 10. Circuit diagram of same balanced-TWPA configuration as in figure 9, highlighting how the convenient separation of the pump and signal tones means the configuration can be transformed relatively simply into an array by connecting the output pump from the first undepleted pump balanced-TWPA into the pump input of the second, and so on, thereby pumping many balanced TWPAs with just a single pump line.

except the second pump tone is now injected at the same input port as the signal, which results in the signal and one of the pump tones being present at one of the output ports, and the idler and other pump tone being present at the other. As with figure 8, this configuration solves the signal-idler contamination with the added advantage of operating a balanced-TWPA in the NP-4WM regime, where the zero-gain gap in the centre of the gain profile is eliminated [24], resulting in an extremely wide and uniform gain profile. Given that the pumps are located at the edges of the gain profile means that they can be easily filtered out using a band-pass filter, hence enabling the full bandwidth of the TWPA to be utilised.

The phase-control technique can be further applied to the DC-3WM regime, with the phase shift for this regime summarised as,

$$\delta_i = \delta_p - \delta_s. \tag{7}$$

Unlike the previous configurations, 180-degree hybrids are used due to the different phase relation in this regime, as shown in figure 12(a). P_{out} of the 180-degree hybrids in this case is given by,

$$P_{\text{out}}^{(\text{Port 1})} = \frac{1}{\sqrt{2}}(P_{\text{in}}^{(\text{Port 1})}e^{-i\frac{\pi}{2}} + P_{\text{in}}^{(\text{Port 2})}e^{-i\frac{\pi}{2}}) \tag{8a}$$

$$P_{\text{out}}^{(\text{Port 2})} = \frac{1}{\sqrt{2}}(P_{\text{in}}^{(\text{Port 1})}e^{-i\frac{\pi}{2}} + P_{\text{in}}^{(\text{Port 2})}e^{-i\frac{3\pi}{2}}), \tag{8b}$$

where P_{in} denotes the input power. Figure 12(b) shows the simulated gain profiles at the output ports of the setup in figure 12(a). The signal and pump are injected into separate input ports and the signal is seperated from the pump and idler tones at the output ports. This not only addresses the signal-idler contamination, but also

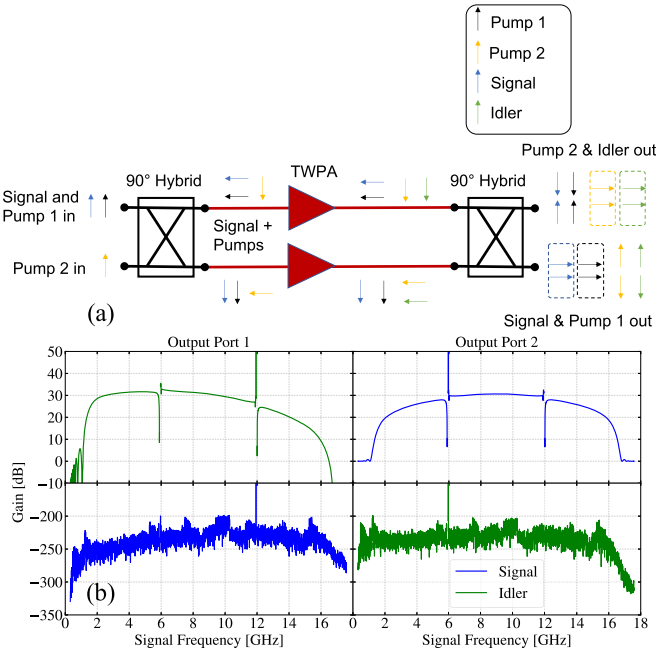

Figure 11. (a) Circuit diagram of a NP-4WM parallel-TWPA with quadrature hybrids. This setup involves injecting the signal and first pump tones into one port of the first hybrid and the second pump tone into the other. Combining the resultant tones at the second hybrid results in the signal and first pump exiting at one port and the second pump and idler exiting at the other. (b) Simulated gain profiles of the output tones at each outputs.

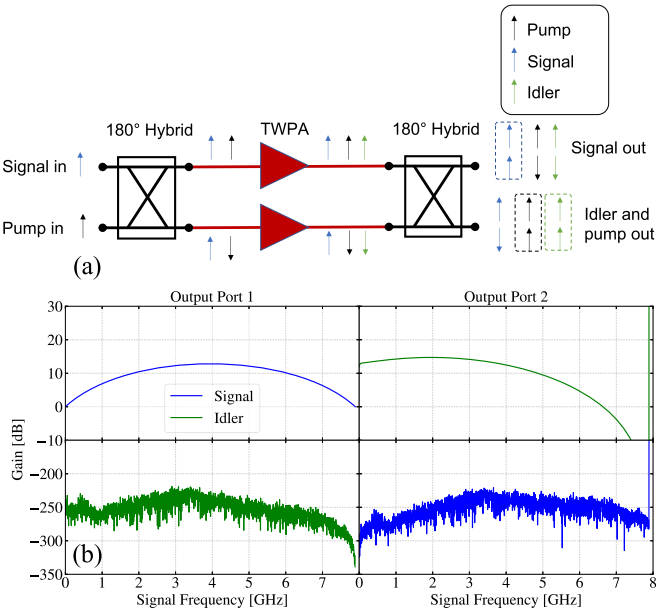

Figure 12. (a) Circuit diagram of a DC-3WM parallel-TWPA with 180-degree hybrids. This setup involves injecting the signal and pump tones into separate ports of the first hybrid, which results in the signals being in-phase relative to each arm and the pumps being in anti-phase. Combining the resultant tones at the second hybrid results in the signal exiting at one port and the pump and idler exiting at the other. (b) Simulated gain profiles of the output tones at each output ports.

provides convenient pump injection and removal schemes for an easy-to-implement experimental setup. This configuration can also be operated in a reverse-isolating mode if the idler is read out instead of the signal, hence this configuration presents an almost-ideal TWPA for many practical applications.

It should be noted that unlike the DP-4WM and NP-4WM modes, the pump tone for a DC-3WM TWPA is located relatively far away from signal amplification band at twice the central frequency, which necessitates a broader bandwidth hybrid coupler. Looking at the gain profiles in figure 12(b) as an example, we note that the central part of the gain profile covers the frequency range 2-6 GHz. The pump tone around 8 GHz means that

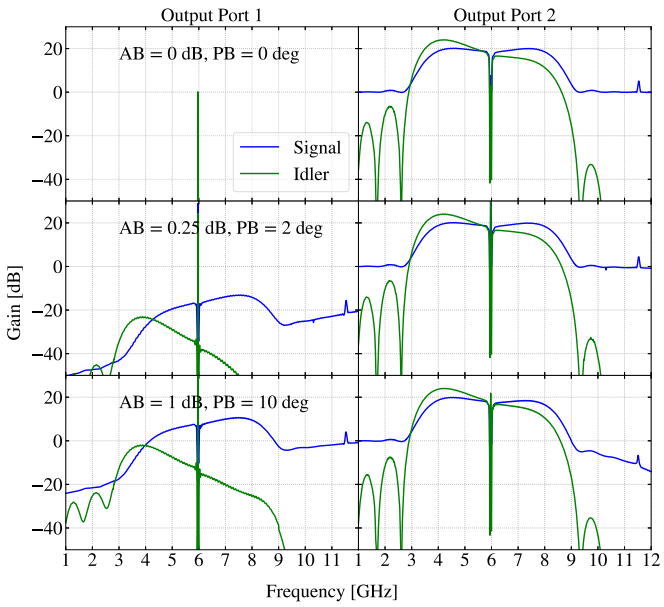

Figure 13. Simulated signal (blue) and idler (green) gain profiles at each output port for the configuration shown in figure 9(a), which are obtained with harmonic balance simulations. The spectra are calculated for three levels of hybrid amplitude and phase imbalances.

the hybrid coupler needs to cover the frequency range 2-8 GHz, which although is wider than for a DP-4WM and NP-4WM balanced-TWPA with the same amplification band, it is still within reasonable limits.

The examples presented above are just a small subset of the many configurations made possible by the balanced-TWPA scheme (there are too many for all configurations to be included in this manuscript), be it using NP-4WM, DP-4WM, or DC-3WM. These configurations can also be applied to KITWPAs, JTWPAs, SQUID-TWPAs, as well as JPAs, which are already widely used in ultra-sensitive cryogenic experiments, stressing the importance of the balanced-architecture.

5. Harmonic balance simulations.

To further validate the feasibility of the proposed balanced-TWPA scheme, we conducted harmonic balance (HB) simulations using the commercial software Keysight Advanced Design System (ADS)®, following the technique described in [35]. The previous analysis in section 4 assumed that the two TWPAs in the balanced-TWPA are identical and that the two hybrids are ideal. In practice, these assumptions may not hold due to fabrication inaccuracies. Here, we investigate the effects of having a pair of non-identical TWPAs or imperfect hybrids with small amplitude imbalance (*AB*) and phase imbalance (*PB*). For these simulations, we focused on the balanced-TWPA configuration shown in figure 9 as example, although the same analysis can be applied to all other configurations.

The following HB simulations use a pair of JTWPA devices, which are nominally identical in design to the JTWPA presented in [5], and comprise a 2000 unit cell Josephson junction embedded transmission line with resonant phase matching (RPM). We opt to use a JTWPA instead of a KITWPA to perform the analysis here as it is much more straightforward to perform HB simulations using ADS with a JTWPA without further complications. Furthermore, the choice of TWPA used here is not crucial and does not influence the conclusions drawn in this section.

5.1. Hybrid Imbalance

The effects of using slightly imbalanced hybrid couplers are illustrated in figure 13, which displays the signal and idler gains at the balanced-TWPA output ports for different *AB* and *PB* values. We considered *AB* and *PB* values ranging from ideal (top panels) to typical (middle panels) and maximum (bottom panels) imbalance, as specified in the data sheet of a commercially available Marki Microwave® QH-0226 quadrature hybrid. The hybrid coupler was simulated using a generic hybrid coupler component from the ADS component libraries and manually adding the *AB* and *PB* values from the QH-0226 datasheet [36]. A critical observation is that the HB simulations produce the same gain spectra as shown in figure 9(b), which aligns with the earlier simulation results assuming ideal hybrids, confirming the methodology we applied earlier.

Recall that the primary function of the balanced-TWPA presented in figure 9 is to effectively separate the strong pump tone from the signal/idler band. As *AB* and *PB* values increase, the signal and idler gains at output port 1 (out-port 1) start to rise, and a weak pump tone appears at output port 2 (out-port 2). This outcome is expected because the non-ideal phase relations of the hybrids mean that the signal and idler (and pump) are no longer fully suppressed at out-port 1 (and out-port 2). However, even with maximum imbalance values (*AB*=1 dB and *PB*=10 °), the signal and idler profiles at out-port 2 remain largely similar, with only a slight asymmetry outside the useful band. The imperfect cancellation of pump tones also appears to have a negligible effect, as indicated by the bottom panels of figure 13, where the pump's amplitude is at a similar level to the peak signal/idler value. Therefore, it would not significantly impact the operation of subsequent microwave components

One way to quantify the effect of the hybrid imbalance is to calculate the change in the signal-to-noise ratio (SNR) at the output ports due to the change in output signal power. If we assume that the noise is unchanged at the output ports, then for the case of AB = 0.25 dB and PB = 2 deg, the output signal at out-port 1 is, in the worst case, about 30 dB weaker than at out-port 2, i.e., 0.1 % of the signal power is diverted to out-port 1, meaning the SNR at out-port 2 is now 99.9 % of the value in the ideal case. For the case of AB = 1 dB and PB = 10 deg, the output signal at out-port 1 is, in the worst case, about 10 dB weaker than at out-port 2, meaning the SNR at out-port 2 is now 90 % of the value in the ideal case. For the AB = 0.25 dB and PB = 2 deg case, the SNR change is very small, further suggesting that the operation of a balanced-TWPA is not limited by typical hybrid imbalance values. Even for the AB = 1 dB and PB = 10 deg case, the drop in the SNR value is still significantly lower than than if the TWPA was replaced by a conventional semiconductor-based amplifier with the same gain performance.

As stated previously, however, this analysis assumes that the noise is unchanged at the output ports, however, it is possible that the balanced-TWPA also diverts the different noise contributions from each tone to separate ports. If the noise contributions are diverted with the same ratios as the tone amplitudes, then it may be that the SNR is unaffected by hybrid imbalance. This final point requires further study.

In conclusion, the use of non-ideal hybrid couplers does not present a significant obstacle to the physical implementation of a balanced-TWPA. These results demonstrate that the configuration exhibits reasonable resilience to hybrid coupler imbalance in both amplitude and phase to a certain degree.

5.2. TWPA imbalance

Next, we investigate the effect of having a pair of non-identical TWPAs. For a TWPA consisting of a series of junctions (or SQUIDs), the primary fabrication tolerance is related to the uniformity of the junction size. This uniformity directly impacts the junction inductance, which controls the gain and phase length of the device. Conversely, for a kinetic inductance TWPA, the main challenge is maintaining the uniformity of the normal-state surface resistivity (ρ_N), which, once again, affects the kinetic inductance, controlling the gain and phase length. Given that the kinetic inductance of a KITWPA is nearly three orders of magnitude weaker than the junction inductance, it's evident that a JTWPA's performance is more sensitive to fabrication inaccuracies. Therefore, for this analysis, we opt to modify the junction inductance to assess the effect of fabrication tolerance on the effectiveness of a balanced-TWPA. The results are presented in figure 14 for the same device shown in figure 9. In this simulation we assume that all the junctions within a single JTWPA have the same junction inductance, L_J, then we modify the difference in L_J between the two JTWPAs, which is quantified as a percentage by the defined parameter,

$$L_{\text{diff}} = \frac{L_J^{(\text{Top})} - L_J^{(\text{Bottom})}}{L_J^{(\text{Top})}} \times 100, \tag{9}$$

where $L_J^{(\text{Top/Bottom})}$ signifies the junction inductance of the top/bottom JTWPA. Similarly to the hybrid imbalance analysis, we observe an increase in signal and idler gains at out-port 1, as well as the appearance of the pump tone at out-port 2, as L_{diff} is increased. Even in the most severe case simulated here, with $L_{\text{diff}} = 1\%$, the signal and idler profiles at the expected out-port 2 remain largely similar, and the pump's amplitude only marginally increases at out-port 1.

This exercise once again demonstrates the feasibility of the balanced-TWPA scheme, at least for this particular configuration. However, it's essential to note that in the most severe case shown here, as well as in the bottom panels of figure 14 from the hybrid imbalance analysis, the signal and idler tones become much stronger at the unwanted out-port 1. This implies that, for a signal/idler separation scheme, more stringent requirements would be necessary for the hybrid and the identicality of the TWPAs. For example, it may require reducing $AB < 0.25$ dB and $PB < 2°$ or $L_{\text{diff}} < 0.1\%$. Therefore, it's important to note that different applications may have varying tolerance requirements, but in most cases, these requirements appear to be within the limits of current technology.

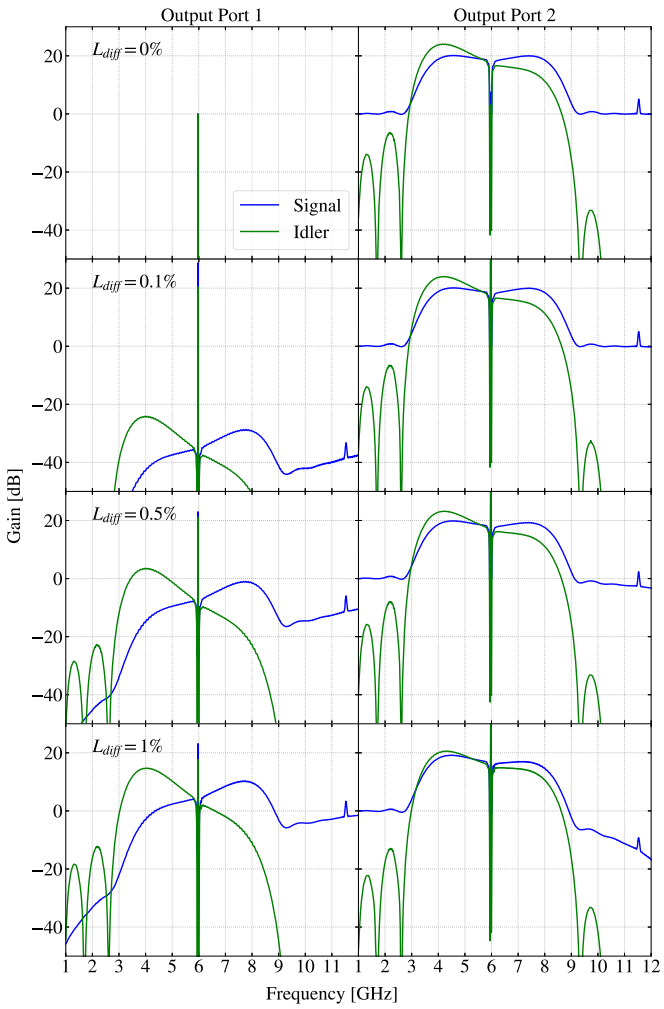

Figure 14. Simulated signal (blue) and idler (green) gain profiles at each output port for the configuration shown in figure 9(a), which have been simulated with harmonic balance simulations. The spectra have been calculated for five different inductance differences, L_{diff}, between the two TWPAs in the balanced-TWPA.

The sensitivity of the balanced-JTWPA's functionality to changes in L_{diff} is not surprising, as the phase velocity is related to the effective wavelength, which, in turn, is related to the inductance per length of the device ($\lambda \propto L^{-\frac{1}{2}}$). A 1% change in L results in approximately a 0.5% change in λ. Since a typical JTWPA device usually has an electrical length of about 300 half-wavelength unit cells, this 1% change leads to a shift in the electrical length of the JTWPA by more than half a wavelength, or 180°, effectively reversing the function of the hybrid. However, the situation is not as dire as it may seem. It just implies that, for this example, operating the balanced-JTWPA in signal-idler separation mode in the DP4WM mode is more challenging. Furthermore, as we argued earlier, the changes in the kinetic inductance of a KITWPA are much weaker than in a JTWPA, suggesting that the balanced-TWPA scheme may be more favourable for KITWPA than JTWPA.

It's important to note that in the DC-3WM mode, the phase length of the TWPA can be easily controlled by the biased DC current. Unlike it's 4WM counterpart, the gain of a DC-3WM TWPA is comparatively less sensitive to the strength of the DC current, however, changes to phase length of the device, on the other hand, are very sensitive to the DC current amplitude. This, therefore, allows us to operate the balanced-TWPA in the DC-3WM mode, enabling external control of the phase length of one of the JTWPA devices by injecting a separate DC current into each TWPA. This ensures that the proper phase relation is maintained for maximum performance. It's worth emphasising that the DC-3WM balanced-TWPA, with separate DC current biasing, represents the best configuration presented in this manuscript (see table 1), as it fulfils all the requirements and addresses all the issues discussed since the beginning of the manuscript. In a way, this configuration of balanced-TWPA can be considered the version that is closest to an ideal amplifier.

Table 1. Summary of balanced-TWPA configurations.

Configuration	Wave mixing	Signal/Idler separation	Simple pump injection	Simple pump removal	Reverse-Isolating mode
Figure 7	DP-4WM	✓[a]	—	✓[a]	—
Figure 8	DP-4WM	✓	—	—	✓
Figure 9	DP-4WM	—	✓	✓	—
Figure 11	NP-4WM	✓	—	—	✓
figure 12	DC-3WM	✓	✓	✓[a]	✓[a]

[a] Functionalities can be re-configured externally to achieve different purposes.

6. Conclusions

In this paper, we have introduced an elegant solution to address the various challenges hindering the widespread use of TWPA technology: a balanced-TWPA architecture that manipulates the phases of the propagating tones to separate them using constructive and destructive interference. This configuration can be easily adjusted to meet different application needs, it offers straightforward operation without imposing logistical burdens on the cryogenic system, and it could resolve issues related to back-amplification and signal/idler contamination. We have provided multiple examples covering TWPAs operating in different wave mixing regimes to demonstrate the functionality of the balanced-TWPA. Furthermore, we have validated our simulations by implementing a HB simulation technique using a commercial software package. Our analysis revealed that the specific requirements for a balanced-TWPA depend on the type of TWPA used and the intended applications, but most configurations fall within current technological capabilities. From our investigations, we identified that a DC-3WM KITWPA with a balanced scheme is the closest to an ideal quantum-noise limited amplifier. We aim to demonstrate the feasibility of the proposed balanced-TWPA experimentally in a subsequent publication, particularly to investigate any practical issues that may arise during physical implementation.

Acknowledgments

The authors would like to thank the European Research Council (ERC) programme under the project number 803 862 (SPA4AstroQIT) for supporting this work. For the purpose of Open Access, the author has applied a CC BY public copyright licence to any Author Accepted Manuscript version arising from this submission. J. Longdens PhD studentship is fully supported by the UK Science and Technology Facilities Council. J. Navarro Montilla's PhD studentship is supported by the UK Science and Technology Facilities Council and the Foley-Bejar Scholarship from Balliol College, Oxford.

Data availability statement

All data that support the findings of this study are included within the article (and any supplementary files).

ORCID iDs

J C Longden https://orcid.org/0009-0005-9519-2547
J Navarro Montilla https://orcid.org/0000-0003-4423-8400
B-K Tan https://orcid.org/0000-0002-6252-9351

References

[1] Eom B H, Day P K, Leduc H G and Zmuidzinas J 2012 A wideband, low-noise superconducting amplifier with high dynamic range *Nat. Phys.* **8** 623–7
[2] Vissers M R, Erickson R P, Ku H S, Vale L, Wu X, Hilton G C and Pappas D P 2016 Low-noise kinetic inductance traveling-wave amplifier using three-wave mixing *Appl. Phys. Lett.* **108** 012601
[3] Planat L, Ranadive A, Dassonneville R, Martinez J P, Leger S, Naud C, Buisson O, Hasch-Guichard W, Basko D M and Roch N 2020 A photonic crystal Josephson traveling wave parametric amplifier *Phys. Rev.*X **10** 021021
[4] Macklin C, O'Brien K, Hover D, Schwartz M E, Bolkhovsky V, Zhang X, Oliver W D and Siddiqi I 2015 A near-quantum-limited Josephson traveling-wave parametric amplifier *Science* **350** 307–10
[5] O'Brien K, Macklin C, Siddiqi I and Zhang X 2014 Resonant phase matching of Josephson junction traveling wave parametric amplifiers *Phys. Rev. Lett.* **113** 157001
[6] White T C *et al* 2015 Traveling wave parametric amplifier with Josephson junctions using minimal resonator phase matching *Appl. Phys. Lett.* **106** 242601

[7] Yaakobi O, Friedland L, Macklin C and Siddiqi I 2013 Parametric amplification in Josephson junction embedded transmission lines *Physical Review B—Condensed Matter and Materials Physics* **87** 144301
[8] Bockstiegel C, Gao J, Vissers M R, Sandberg M, Chaudhuri S, Sanders A, Vale L R, Irwin K D and Pappas D P 2014 Development of a broadband NbTiN traveling wave parametric amplifier for MKID readout *Journal of Low Temperature Physics* vol 176 (Springer) pp 476–82
[9] Chaudhuri S, Li D, Irwin K D, Bockstiegel C, Hubmayr J, Ullom J N, Vissers M R and Gao J 2017 Broadband parametric amplifiers based on nonlinear kinetic inductance artificial transmission lines *Appl. Phys. Lett.* **110** 152601
[10] Goldstein S, Kirsh N, Svetitsky E, Zamir Y, Hachmo O, De Oliveira C E M and Katz N 2020 Four wave-mixing in a microstrip kinetic inductance travelling wave parametric amplifier *Appl. Phys. Lett.* **116** 152602
[11] Shu S, Klimovich N, Eom B H, Beyer A D, Thakur R B, Leduc H G and Day P K 2021 Nonlinearity and wide-band parametric amplification in a (Nb,Ti)N microstrip transmission line *Physical Review Research* **3** 1–9
[12] Malnou M, Vissers M R, Wheeler J D, Aumentado J, Hubmayr J, Ullom J N and Gao J 2020 A three-wave mixing kinetic inductance traveling-wave amplifier with near-quantum-limited noise performance *PRX Quantum* **2** 010302
[13] Noroozian O 2020 *Cycle 5 NRAO ALMA Development Study Report Technology Development of Quantum-Limited , Ultra-Wideband RF Amplifiers for ALMA : A 65-150 GHz Test Case*
[14] Zobrist N *et al* 2019 Wide-band parametric amplifier readout and resolution of optical microwave kinetic inductance detectors *Appl. Phys. Lett.* **115** 042601
[15] Che G, Gordon S, Day P, Groppi C, Jackson R, Mani H, Mauskopf P, Surdi H, Trichopoulos G and Underhill M 2017 *A Superconducting Phase Shifter and Traveling Wave Kinetic Inductance Parametric Amplifier for W-Band Astronomy*
[16] Backes K M *et al* 2021 A quantum enhanced search for dark matter axions *Nature* **590** 238–42
[17] Kutlu C ,, Van Loo A F, Uchaikin S V, Matlashov A N, Lee D, Oh S, Kim J, Chung W, Nakamura Y and Semertzidis Y K 2021 Characterization of a flux-driven Josephson parametric amplifier with near quantum-limited added noise for axion search experiments *Superconductor Science and Technology* **34** 085013
[18] Braine T *et al* 2020 Extended search for the invisible axion with the axion dark matter experiment *Phys. Rev. Lett.* **124** 101303
[19] Fasolo L, Greco A, Enrico E, Illuminati F, Lo Franco R, Vitali D and Livreri P 2021 Josephson traveling wave parametric amplifiers as non-classical light source for microwave quantum illumination *Measurement: Sensors* **18** 100349
[20] Ranzani L, Bal M, Fong K C, Ribeill G, Wu X, Long J, Ku H S, Erickson R P, Pappas D and Ohki T A 2018 Kinetic inductance traveling-wave amplifiers for multiplexed qubit readout *Appl. Phys. Lett.* **113** 242602
[21] Gonzalez-Zalba M F, de Franceschi S, Charbon E, Meunier T, Vinet M and Dzurak A S 2021 Scaling silicon-based quantum computing using CMOS technology: State-of-the-art, Challenges and Perspectives *Nat Electron* **4** 872–884
[22] Tan B K, Boussaha F, Chaumont C, Longden J and Navarro Montilla J 2022 Engineering the thin film characteristics for optimal performance of superconducting kinetic inductance amplifiers using a rigorous modelling technique *Open Research Europe* **2** 88
[23] Winkel P *et al* 2019 Non-degenerate parametric amplifiers based on dispersion engineered Josephson junction arrays *Phys. Rev. Appl.* **13** 024015
[24] Longden J C and Tan B K 2024 Non-degenerate-pump four-wave mixing kinetic inductance travelling-wave parametric amplifiers *Engineering Research Express* **6** 015068
[25] Gaydamachenko V, Kissling C, Dolata R and Zorin A B 2022 Numerical analysis of a three-wave-mixing Josephson traveling-wave parametric amplifier with engineered dispersion loadings *J Appl. Phys.* **132** 154401
[26] Tan B K and Longden J C 2023 *Parallel parametric devices. Patent Application* UK2311659.3
[27] Westig M P and Klapwijk T M 2018 Josephson parametric reflection amplifier with integrated directionality *Phys. Rev. Appl.* **9** 064010
[28] Castellanos-Beltran M A and Lehnert K W 2007 Widely tunable parametric amplifier based on a superconducting quantum interference device array resonator *Appl. Phys. Lett.* **91** 83509
[29] Stehlik J, Liu Y Y, Quintana C M, Eichler C, Hartke T R and Petta J R 2015 Fast charge sensing of a cavity-coupled double quantum dot using a josephson parametric amplifier *Phys. Rev. Appl.* **4** 014018
[30] Roy T, Kundu S, Chand M, Vadiraj A M, Ranadive A, Nehra N, Patankar M P, Aumentado J, Clerk A A and Vijay R 2015 Broadband parametric amplification with impedance engineering: Beyond the gain-bandwidth product *Appl. Phys. Lett.* **107** 262601
[31] Kaufman R *et al* 2023 Josephson parametric amplifier with chebyshev gain profile and high saturation *Phys. Rev. Appl.* **20** 054058
[32] Longden J C 2024 Development of Superconducting Thin Film Travelling-Wave Parametric Amplifiers *PhD Thesis* University of Oxford
[33] Chattopadhyay G, Rice F, Miller D, LeDuc H G and Zmuidzinas J 1999 A 530-GHz balanced mixer *IEEE Microw. Guid. Wave Lett.* **9** 467–9
[34] Tan B K and Yassin G 2017 Planar microstrip coupler with enhanced power coupling *Electron. Lett* **53** 34–6
[35] Sweetnam T, Banys D, Gilles V, McCulloch M A and Piccirillo L 2022 Simulating the behaviour of travelling wave superconducting parametric amplifiers using a commercial circuit simulator *Superconductor Science and Technology* **35** 095011
[36] Marki Microwave. *QH-0226 3 dB Quadrature Hybrid*, 2020.